Modern Physics Letters B
2050076 (15 pages)

DOI: 10.1142/S0217984920500761

World Scientific
www.worldscientific.com

Localized waves and interaction solutions to an extended $(3+1)$-dimensional Kadomtsev–Petviashvili equation

Han-Dong Guo and Tie-Cheng Xia*

Department of Mathematics, Shanghai University, Shanghai 200444, China
**xiatc@shu.edu.cn*

Wen-Xiu Ma

Department of Mathematics, Zhejiang Normal University, Jinhua 321004, Zhejiang, China
Department of Mathematics, King Abdulaziz University, Jeddah, Saudi Arabia
International Institute for Symmetry Analysis and Mathematical Modelling, Department of Mathematical Sciences, North-West University, Mafikeng Campus, Private Bag X2046, Mmabatho 2735, South Africa

Received 21 July 2019
Revised 5 October 2019
Accepted 11 October 2019
Published 2 January 2020

In this paper, an extended $(3+1)$-dimensional Kadomtsev–Petviashvili (KP) equation is studied via the Hirota bilinear derivative method. Soliton, breather, lump and rogue waves, which are four types of localized waves, are obtained. N-soliton solution is derived by employing bilinear method. Then, line or general breathers, two-order line or general breathers, interaction solutions between soliton and line or general breathers are constructed by complex conjugate approach. These breathers own different dynamic behaviors in different planes. Taking the long wave limit method on the multi-soliton solutions under special parameter constraints, lumps, two- and three-lump and interaction solutions between dark soliton and dark lump are constructed, respectively. Finally, dark rogue waves, dark two-order rogue waves and related interaction solutions between dark soliton and dark rogue waves or dark lump are also demonstrated. Moreover, dynamical characteristics of these localized waves and interaction solutions are further vividly demonstrated through lots of three-dimensional graphs.

Keywords: Hirota bilinear method; rogue wave; lump; breather; interaction solution.

1. Introduction

Nonlinear evolution equations (NLEEs) have been used to describe many nonlinear phenomena in the nature, such as fluid mechanics, plasma physics, optical fibers and solid state physics.[1–3] Among the NLEEs, (KP)-type equations have been regarded

*Corresponding author.

as the models to describe some nonlinear phenomena in plasmas and fluids.[4,5] Some researchers have proposed the following (3 + 1)-dimensional generalized KP equation[6,7] in recent years:

$$(u_t + k_1 u u_x + k_2 u_{xxx})_x + k_3 u_{xx} + k_4 u_{yy} + k_5 u_{zz} + k_6 u_{xy} + k_7 u_{xz} + k_8 u_{yz} = 0\,. \tag{1}$$

Equation (1) models the evolution of long water waves and small-amplitude surface waves with the weak nonlinearity, weak dispersion and weak perturbation in a fluid. The coefficients k_i $(1 \leq i \leq 8)$ are all parameters which represent different physical meanings.

Multi-soliton solutions and multi-periodic wave solutions for Eq. (1) have been received by virtue of the binary Bell polynomials and Riemann theta function method.[6] Bright breather, lump and rogue wave solutions for Eq. (1) have been studied via the Hirota method.[7] Special cases of Eq. (1) have been explored in physical sciences such as the (1 + 1)-dimensional KdV equation[8] and generalized KP equation.[9]

Letting $k_4 = k_5$, $k_3 = k_6 = k_7 = k_8 = 0$, Eq. (1) has been reduced to a (3 + 1)-dimensional generalized KP equation.[10]

$$(u_t + k_1 u u_x + k_2 u_{xxx})_x + k_4 (u_{yy} + u_{zz}) = 0\,, \tag{2}$$

which can describe many nonlinear phenomena in fluid dynamics. Soliton, rogue wave and interaction solutions for Eq. (2) have been derived via the Bell polynomials.

In recent decades, more and more attention has been paid to the construction of exact solutions of NLEEs. For a given nonlinear system, Hirota method is an effective and direct method to seek the corresponding explicit solutions. Soliton, lump, breather and rogue wave, as four types of localized wave solutions, have aroused great interest in both theories and experiments.

Solitons have been seen as the localized waves in certain directions.[10] Breathers demonstrate themselves as a localized spatial or temporal structure that exhibit oscillatory behavior.[11,12] Rogue waves are considered as the spontaneous nonlinear waves whose amplitudes are larger than the surrounding backgrounds and have been proved to be a kind of the rational solutions localized in both space and time.[13–15] Lump solutions, another kind of the rational solutions, have been found to be localized in all directions of the space.[16,17]

When $k_1 = \sigma, k_2 = 1, k_3 = \alpha, k_4 = \beta, k_5 = \gamma, k_i = 0$ $(6 \leq i \leq 8)$, Eq. (1) is reduced to

$$(u_t + \sigma u u_x + u_{xxx})_x + \alpha u_{xx} + \beta u_{yy} + \gamma u_{zz} = 0\,, \tag{3}$$

which models nonlinear wave in liquid containing gas bubbles. Bäuklund transformations, infinite conservation laws and periodic wave solutions of Eq. (3) are explored by using the Bell polynomial approach.[18]

If setting $\sigma = 6, \beta = \pm 1$, when $\alpha = \gamma = 0$ or $\alpha = -\gamma, z = x$, Eq. (3) is reduced to classical KP equation that can model the water waves of long wavelength with the weakly nonlinear restoring forces and frequency dispersion, waves in the ferromagnetic media, and $(2+1)$-dimensional matter-wave pulses in the Bose–Einstein condensates.[19] Higher-dimensional NLEEs have been proposed for that they can describe the nonlinear phenomena more accurately than those lower-dimensional ones.[20]

As far as we know, the breather, lump and rogue wave for Eq. (3) have not been studied. So, the goal of this paper is to explore four types of localized waves and interaction solutions among them to Eq. (3) by virtue of the method applied in Refs. 21–23. N-soliton solutions are derived according to the Hirota bilinear approach in Sec. 2. Then, the breathers and interaction solutions are obtained by taking complex conjugate of the parameters. Finally, the lumps, rogue waves and interaction solutions between localized waves are also derived by applying long wave limit method on multi-soliton solutions. In particular, the rich dynamic phenomena of the interaction solutions between localized waves are also studied in detail in addition to obtaining the four basic localized waves. Section 3 is a short conclusion.

2. Localized Wave and Interaction Solutions

2.1. *The N-soliton solutions*

Equation (3) can be mapped into bilinear form[24]

$$(D_x D_t + D_x^4 + \alpha D_x^2 + \beta D_y^2 + \gamma D_z^2) f \cdot f = 0\,, \tag{4}$$

under the transformation

$$u = \frac{12}{\sigma}\big(\ln f\big)_{xx}\,, \tag{5}$$

where $f = f(x, y, z, t)$ and the bilinear derivative operators are defined by

$$\begin{aligned} D_x^l D_y^m D_z^n D_t^p (f \cdot g) = {} & \left(\frac{\partial}{\partial x} - \frac{\partial}{\partial x'}\right)^l \left(\frac{\partial}{\partial y} - \frac{\partial}{\partial y'}\right)^m \left(\frac{\partial}{\partial z} - \frac{\partial}{\partial z'}\right)^n \\ & \times \left(\frac{\partial}{\partial t} - \frac{\partial}{\partial t'}\right)^p f(x, y, z, t) g(x', y', z', t')|_{x'=x, y'=y, z'=z, t'=t}. \end{aligned} \tag{6}$$

It is quite evident that $u = u\big(x, y, z, t\big)$ is a solution of Eq. (3) under the transformation (5), if and only if f solves Eq. (4).

Substituting

$$u = \exp^{\eta_i}, \quad \eta_i = k_i(x + p_i y + q_i z + \omega_i t) + \eta_i^0\,, \tag{7}$$

into the linear terms of Eq. (3), and solving the resulting equation for ω_i we obtain the dispersion relation as

$$\omega_i = -(\alpha + k_i^2 + \beta p_i^2 + \gamma q_i^2), \quad i = 1, 2, \ldots, N\,, \tag{8}$$

and hence the wave variable η_i becomes

$$\eta_i = k_i(x + p_i y + q_i z - (\alpha + k_i^2 + \beta p_i^2 + \gamma q_i^2)t) + \eta_i^0, \quad i = 1, 2, \ldots, N\,. \tag{9}$$

When $N = 1$, supposing $f = 1 + \exp^{\eta_1}$, then one-soliton solution for Eq. (3) is obtained by transformation (5). When $N = 2$, supposing $f = 1 + \exp^{\eta_1} + \exp^{\eta_2} + A_{12}\exp^{\eta_1+\eta_2}$. Substituting f into Eq. (4), and solving for the phase shift A_{ij}, we find

$$A_{ij} = \frac{\beta(p_i - p_j)^2 + \gamma(q_i - q_j)^2 - 3(k_i - k_j)^2}{\beta(p_i - p_j)^2 + \gamma(q_i - q_j)^2 - 3(k_i + k_j)^2}, \quad 1 \le i < j \le 3\,. \tag{10}$$

When $N = 3$, supposing $f = 1+\exp^{\eta_1}+\exp^{\eta_2}+\exp^{\eta_3}+A_{12}\exp^{\eta_1+\eta_2}+A_{13}\exp^{\eta_1+\eta_3}+A_{23}\exp^{\eta_2+\eta_3}+A_{123}\exp^{\eta_1+\eta_2+\eta_3}$, analogously we derive $A_{123} = A_{12}A_{13}A_{23}$ which is a condition for the integrability of the three-soliton.

Recursively, we derive N-soliton solutions of Eq. (3), which can be obtained by substituting

$$f = \sum_{\mu=0,1} \exp\left(\sum_{i=1}^{N} \mu_i \eta_i + \sum_{1\le i<j}^{N} \mu_i \mu_j \ln(A_{ij})\right), \tag{11}$$

into Eq. (4) via the simplified Hirota method, and

$$\begin{aligned} &\eta_i = k_i(x + p_i y + q_i z - (\alpha + k_i^2 + \beta p_i^2 + \gamma q_i^2)t) + \eta_i^0, \quad i = 1, 2, \ldots, N\,, \\ &A_{ij} = \frac{\beta(p_i - p_j)^2 + \gamma(q_i - q_j)^2 - 3(k_i - k_j)^2}{\beta(p_i - p_j)^2 + \gamma(q_i - q_j)^2 - 3(k_i + k_j)^2}, \quad 1 \le i < j \le N\,, \end{aligned} \tag{12}$$

where k_i, p_i, q_i and η_i^0 are arbitrary constants, $\sum_{\mu=0,1}$ is the summation with possible combinations of $\mu_i = 0, 1$ $(i = 1, 2, \ldots, N)$.

To demonstrate the dynamic phenomena of the soliton solutions, we take $N = 1, 2, 3$ for example. Then, the explicit one-, two- and three-soliton solutions can be obtained with the following parameters:

$$\begin{aligned} &\alpha = 1, \quad \beta = \gamma = -1, \ \sigma = 6\,, \\ &N = 1, \quad k_1 = 1, \quad p_1 = 1, \quad q_1 = 2, \quad \eta_1^0 = 0\,, \\ &N = 2, \quad k_1 = 1, \quad p_1 = 2, \quad q_1 = 1, \quad k_2 = 1, \quad p_2 = 1\,, \\ &q_2 = 2, \quad \eta_1^0 = \eta_2^0 = 0\,, \\ &N = 3, \quad k_1 = 1, \quad p_1 = 0.5, \quad q_1 = 2, \quad k_2 = 1, \quad p_2 = 1\,, \\ &q_2 = 1, \quad k_3 = 1, \quad p_3 = 3, \quad q_3 = 1, \quad \eta_1^0 = \eta_2^0 = \eta_3^0 = 0\,. \end{aligned} \tag{13}$$

It is visually shown that the collisions are elastic, which can be seen in Fig. 1. After the collision of the solitons, their speeds and shapes are kept unchanged, but the phases have a change. When σ is positive or negative, bright and dark solitons are obtained, respectively. In addition, the amplitude increases with σ decreasing, hence amplitude of the solitons is negative correlation with σ.

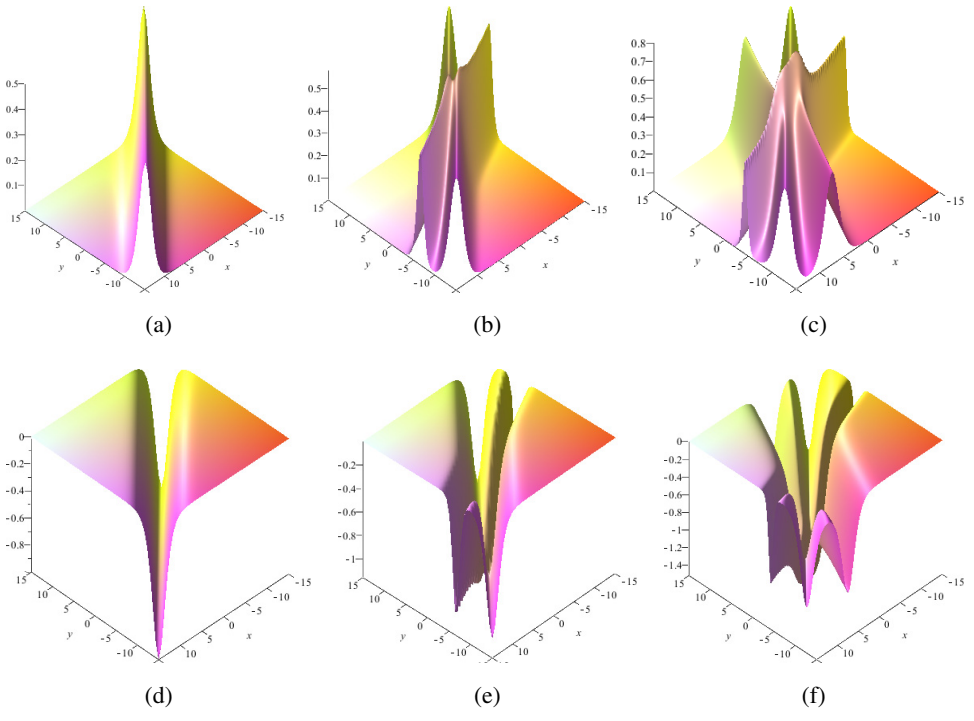

Fig. 1. (Color online) (a–c): three dimension graphs of bright one-, two- and three-soliton solutions of Eq. (3) at (x, y) plane by choosing $z = 0, t = 0$; (d–f): the corresponding dark soliton solutions only with $\sigma = -3$ in Eq. (13).

2.2. *The breather solutions*

By taking complex conjugate approach for arbitrary parameters in Eq. (11), breather solutions of the extended KP Eq. (3) can be constructed and they exhibit different dynamic phenomena on different planes.

When $N = 2$, letting the parameters in Eq. (11) satisfy the following constraints:

$$k_1 = k_2^* = ai, \quad p_1 = p_2^* = c + di, \quad q_1 = q_2 = b, \quad (i^2 = -1)\,. \tag{14}$$

Now, f in Eq. (11) can be rewritten as

$$f = 1 + 2\exp(-ad(y - 2\beta ct))\cos(a(x + cy + bz + (a^2 - \gamma b^2 - \beta c^2 + \beta d^2 - \alpha)t)) + \left(1 - \frac{3a^2}{\beta d^2}\right)\exp(-2ad(y - 2\beta ct))\,. \tag{15}$$

Then, the general breathers can be derived by choosing suitable parameters in Eq. (14), whose dynamical behaviors are demonstrated in Fig. 2. These breathers propagate along the axis with stable shape, amplitude and velocity. The line breather in (x, z) plane can be constructed with the same parameters, whose three-dimensional graphs are demonstrated in Fig. 3. These periodic line waves are line breathers, whose limiting cases can generate the fundamental line rogue waves.

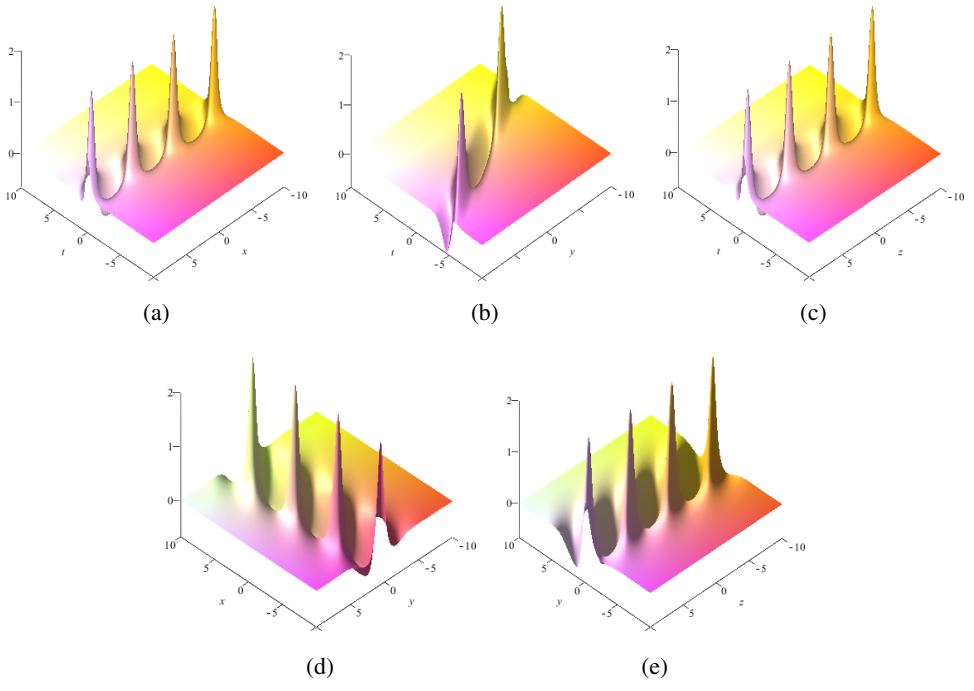

Fig. 2. (Color online) General breathers of Eq. (3) in different planes with parameters constrained by $a = b = c = d = 1, \alpha = 1, \beta = \gamma = -1, \sigma = 6, \eta_1^0 = \eta_2^0 = 0$.

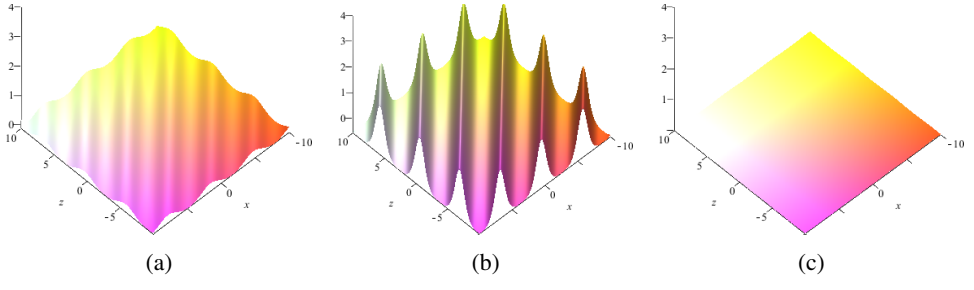

Fig. 3. (Color online) Line breathers of Eq. (3) in (x, z) plane at $y = 0$: (a) $t = -1$, (b) $t = 0$ and (c) $t = 3$. The parameters are the same as in Fig. 2.

The line breathers originate from a plane and then they gradually reach the maximum amplitude 1.332 at $t = 0$. Finally, they gradually return to the original state.

When σ increases, amplitude of general or line breather decreases, but periodicity keeps unchanged. The shape, amplitude and periodicity are all influenced and controlled by the parameters α, β and γ.

In the case of $N = 3$, we derive interaction solutions between solitons and breathers by choosing suitable parameters. When the parameters of Eq. (11) and

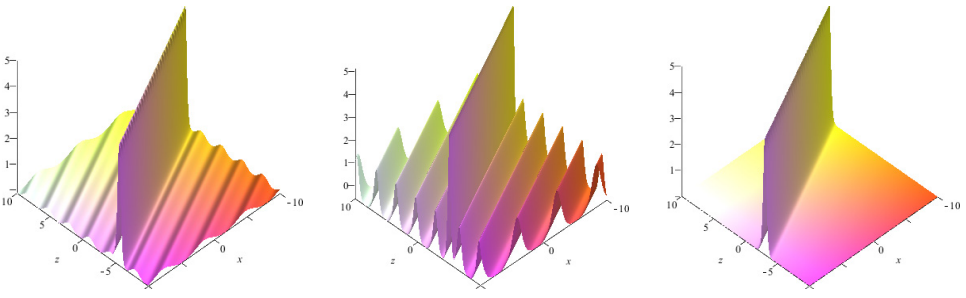

(a) (b) (c)

Fig. 4. (Color online) The spatial structure of interaction solutions between soliton and line breather in (x, z) plane at $y = 0$, (a) $t = -0.5$, (b) $t = 0$ and (c) $t = 2$. The parameters are constrained in Eq. (16).

coefficients of Eq. (3) are selected as follows:

$$\begin{aligned} &k_1 = k_3^* = i, \quad p_1 = p_3^* = 2 + i, \quad (i^2 = -1), \quad q_1 = q_3 = 2\,, \\ &k_2 = 3, \quad p_2 = 2, \quad q_2 = 2, \quad \eta_1^0 = \eta_2^0 = \eta_3^0 = 0, \quad \sigma = 6\,, \\ &\alpha = 1, \quad \beta = \gamma = -1\,, \end{aligned} \tag{16}$$

the expression of f in Eq. (11) can be adduced that

$$\begin{aligned} f = {} & 1 + \exp(3x + 6y + 6z - 6t) + 4\exp(-2y - 8t) + 4\exp(3x + 4y + 6z - 14t) \\ & + 2\exp(-y - 4t)\cos(x + 2y + 2z + 7t) \\ & + \frac{410}{853}\exp(3x + 5y + 6z - 10t)\cos(x + 2y + 2z + 7t) \\ & + \frac{1656}{853}\exp(3x + 5y + 6z - 10t)\sin(x + 2y + 2z + 7t)\,. \end{aligned} \tag{17}$$

Then, we receive two categories of interaction solutions between soliton and line breather or general breather by choosing suitable parameters in Eq. (11). The interaction phenomena and dynamical behaviors can be seen in Figs. 4 and 5. From Fig. 4, it can be seen that the amplitude of the interaction solution reaches maximum 5.13 at $t = 0$. The soliton divides the line breather into two parts. The line breather disappears and soliton will be left alone as time goes by. Obviously, the periodicity and propagation directions of these interaction solutions between soliton and general breather are distinct with each other from Fig. 5.

In the case of $N = 4$, interaction solutions between breathers are derived by choosing suitable parameters. The function f in the four-soliton solution u has the following form:

$$\begin{aligned} f = {} & 1 + \exp^{\eta_1} + \exp^{\eta_2} + \exp^{\eta_3} + \exp^{\eta_4} + A_{12}\exp^{\eta_1+\eta_2} + A_{13}\exp^{\eta_1+\eta_3} \\ & + A_{14}\exp^{\eta_1+\eta_4} + A_{23}\exp^{\eta_2+\eta_3} + A_{24}\exp^{\eta_2+\eta_4} + A_{34}\exp^{\eta_3+\eta_4} \\ & + A_{12}A_{13}A_{23}\exp^{\eta_1+\eta_2+\eta_3} + A_{12}A_{14}A_{24}\exp^{\eta_1+\eta_2+\eta_4} \end{aligned}$$

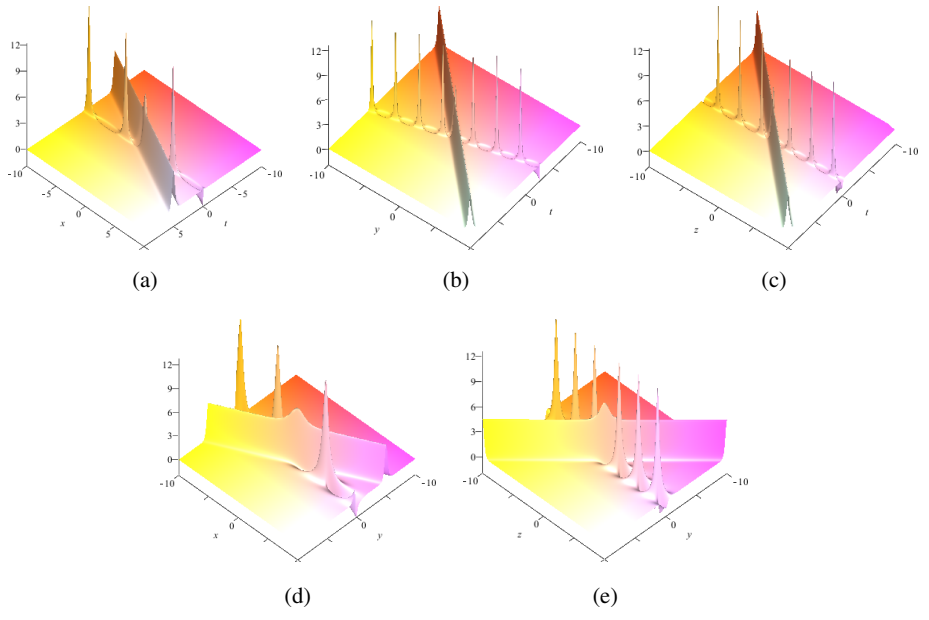

Fig. 5. (Color online) The spatial structure of interaction solutions between soliton and general breathers in different planes. The parameters are constrained in Eq. (16) only p_1 should be replaced with $2+3i$.

$$+A_{13}A_{14}A_{34}\exp^{\eta_1+\eta_3+\eta_4}+A_{23}A_{24}A_{34}\exp^{\eta_2+\eta_3+\eta_4}$$
$$+A_{12}A_{13}A_{14}A_{23}A_{24}A_{34}\exp^{\eta_1+\eta_2+\eta_3+\eta_4}, \tag{18}$$

with the parameters in accordance with Eq. (12). The parameters in Eq. (18) are set as follows:

$$\begin{aligned}
&k_1=k_2^*=i, \quad k_3=k_4^*=2i, \quad p_1=p_2^*=1+i,\\
&p_3=p_4^*=2+i, \quad (i^2=-1),\\
&q_1=q_2=1, \quad q_3=q_4=2, \quad \eta_j^0=0,\\
&(j=1,2,3,4), \quad \sigma=6, \quad \alpha=1, \quad \beta=\gamma=-1.
\end{aligned} \tag{19}$$

Similar to the case of $N=3$, two kinds of two-order breathers are demonstrated in Figs. 6–7. In Fig. 6, as t goes on, we can observe that one breather fissions into two-order smaller period breathers. In Fig. 7, the two line breathers emerge from a constant plane and the amplitude reaches to the maximum 3.649 at $t=0$ and then they tend to the original plane. The interaction solutions of two-soliton and general breather can be obtained by selecting another set of suitable parameters. Dynamic phenomena can be seen in Fig. 8 and the parameters are constrained as: $k_1=k_2^*=i, p_1=p_2^*=1+3i, q_1=q_2=1, k_3=1, p_3=2, q_3=3, k_4=2, p_4=1, q_4=4, \sigma=6, \alpha=1, \beta=\gamma=-1$.

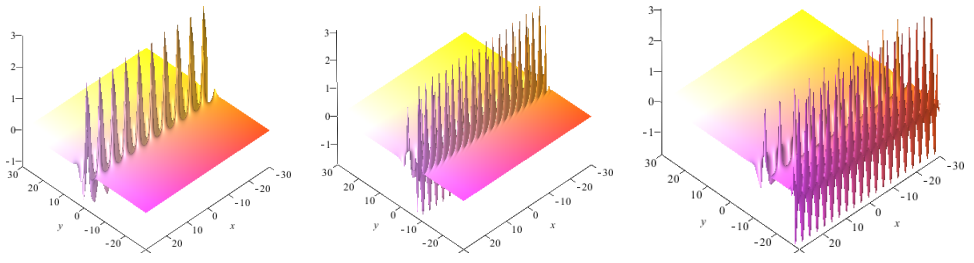

Fig. 6. (Color online) Interaction phenomenon of two-order general breathers in (x, y) plane: (a) $t = 0$, (b) $t = 2$ and (c) $t = 7$. Parameters are given in Eq. (19).

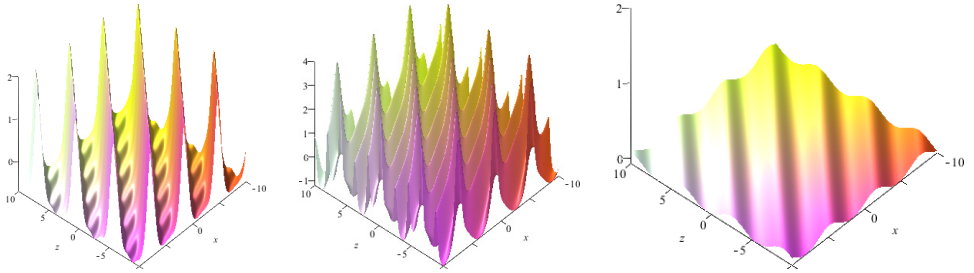

Fig. 7. (Color online) Interaction phenomenon of two-order line breathers in (x, z) plane: (a) $t = -0.5$, (b) $t = 0$ and (c) $t = 2$ and parameters are given in Eq. (19).

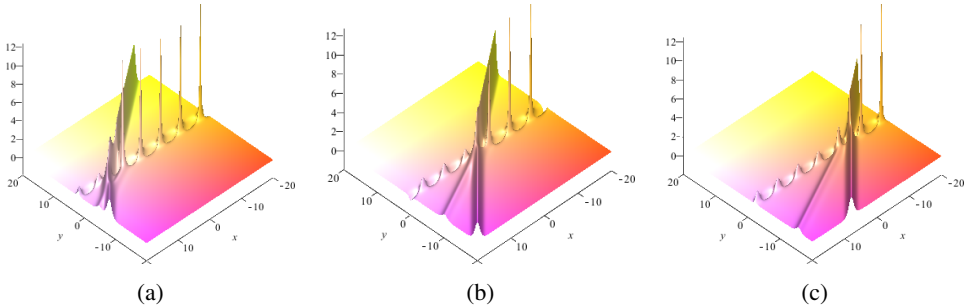

Fig. 8. (Color online) Interaction phenomenon of two-soliton and general breathers in (x, y) plane at $z = 0$: (a) $t = -1$, (b) $t = 0$ and (c) $t = 1$.

2.3. *The lump solutions*

In this section, we will derive lump solutions by using long wave limit method[25] on multi-soliton solutions. There are many kinds of excitation phenomena in physics, for example, dromions, ring-shape and bubble-like excitations for self-dual Yang–Mills system are obtained by Lou.[26] When $N = 2$, we can construct lump solutions

by choosing appropriate parameters in Eq. (11) as follows:

$$N = 2, \quad k_1 = l_1\epsilon, \quad k_2 = l_2\epsilon, \quad \eta_1^0 = \eta_2^{0*} = i\pi\,, \tag{20}$$

it thus transpires that

$$f = (\theta_1\theta_2 + \theta_0)l_1 l_2\epsilon^2 + O(\epsilon^3)\,. \tag{21}$$

By taking the limit of $\epsilon \to 0$ in Eq. (21), it follows:

$$u = -\frac{12(\theta_1^2 + \theta_2^2 - 2\theta_0)}{\sigma(\theta_1\theta_2 + \theta_0)^2}\,, \tag{22}$$

with

$$\begin{aligned} \theta_0 &= \frac{12}{\beta(p_1 - p_2)^2 + \gamma(q_1 - q_2)^2}\,, \\ \theta_i &= x + p_i y + q_i z - (\alpha + \beta p_i^2 + \gamma q_i^2)t \quad (i = 1, 2)\,. \end{aligned} \tag{23}$$

If setting $p_2 = p_1^*, q_2 = q_1^*$, the solution u in Eq. (22) is obviously nonsingular. In order to demonstrate the characteristics of the solution (22), we assume $p_1 = a_1 + ib_1, q_1 = a_2 + ib_2$ and a_1, a_2, b_1, b_2 are all real constants.

When $a_1 \neq 0$, the trajectory can be defined along the path $[x(t), y(t)]$ as follows:

$$\begin{aligned} x + a_1 y + a_2 z - (\alpha + \beta(a_1^2 - b_1^2) + \gamma(a_2^2 - b_2^2))t = 0\,, \\ a_2 y + b_2 z - 2(\beta a_1 b_1 + \gamma a_2 b_2)t = 0\,. \end{aligned} \tag{24}$$

Meanwhile, formula (22) can be rewritten as

$$u = -\frac{24}{\sigma}\frac{(x' + a_1 y' + a_2 z')^2 - (b_1 y' + b_2 z')^2 + \frac{3}{\beta b_1^2 + \gamma b_2^2}}{\left[(x' + a_1 y' + a_2 z')^2 + (b_1 y' + b_2 z')^2 - \frac{3}{\beta b_1^2 + \gamma b_2^2}\right]^2}\,, \tag{25}$$

where

$$x' = x + [\beta(a_1^2 + b_1^2) + \gamma(a_2^2 + b_2^2) - \alpha]t, \quad y' = y - 2\beta a_1 t, \quad z' = z - 2\gamma a_2 t\,.$$

From Ref. 27, it can be adduced that the solution u in Eq. (25) is a constant and keeps the permanent lump conditions in the process of propagating along the trajectory (24) with the condition $\beta b_1^2 + \gamma b_2^2 < 0$. This solution is decaying as $O(1/x^2, 1/y^2, 1/z^2)$ for $|x|, |y|, |z| \to \infty$ and moving with the velocity $v_x = -[\beta(a_1^2 + b_1^2) + \gamma(a_2^2 + b_2^2) - \alpha], v_y = 2\beta a_1 t, v_z = 2\gamma a_2 t$.

The spatial structures of lumps are visually demonstrated in Fig. 9 and localized in all directions. When σ increases, amplitude of the lump decreases, and location of the peak remains unchanged; when β or γ increases, lump wave's amplitude increases and meanwhile it becomes tall and slender, but location of peak remain unchanged; when β increases, amplitude and peak of the lump remains unchanged.

In the case of $N = 3$, by applying the long wave limit approach on the three-soliton solution, we can derive interaction solutions between solitons and lumps in different planes. We constraint the parameters similar in Eq. (20)

$$N = 3, \quad k_1 = l_1\epsilon, \quad k_2 = l_2\epsilon, \quad k_3 = k_3, \quad \eta_1^0 = \eta_2^{0*} = i\pi, \quad \eta_3^0 = \eta_3^0\,, \tag{26}$$

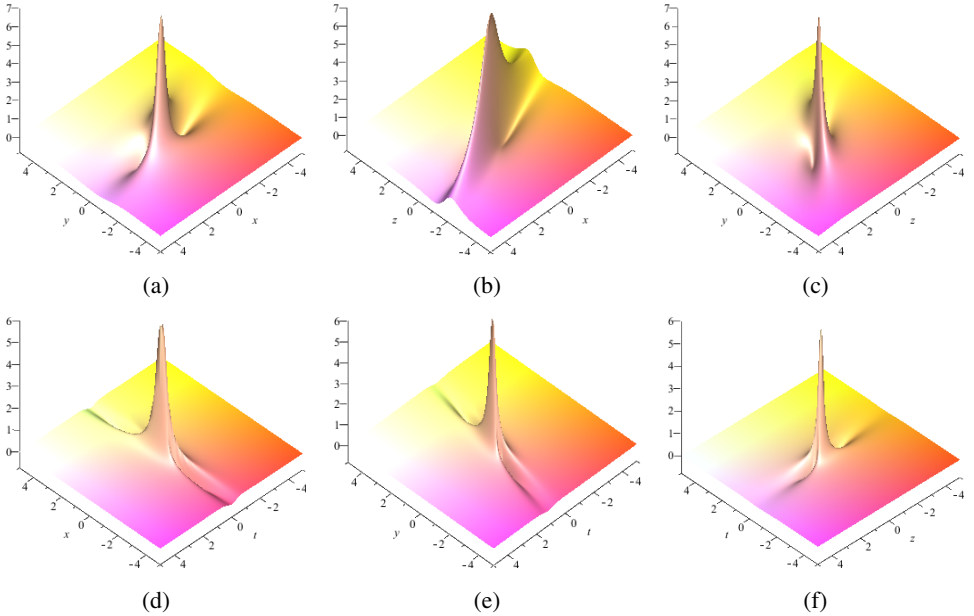

Fig. 9. (Color online) The lump solutions in different planes with $a_1 = 1, b_1 = 2, a_2 = 2, b_2 = 1, \sigma = 6, \alpha = 1, \beta = \gamma = -1$ in Eq. (22).

and taking limit $\epsilon \to 0$, it then follows:

$$f = (\theta_1\theta_2 + a_{12})l_1l_2 + (\theta_1\theta_2 + a_{12} + a_{13}\theta_2 + a_{23}\theta_1 + a_{13}a_{23})l_1l_2e^{\eta_3}\,, \tag{27}$$

where

$$\begin{aligned} a_{12} &= \frac{12}{\beta(p_1 - p_2)^2 + \gamma(q_1 - q_2)^2}\,, \\ \theta_i &= x + p_i y + q_i z - (\alpha + \beta p_i^2 + \gamma q_i^2)t\,, \\ a_{i3} &= \frac{12k_3}{\beta(p_i - p_3)^2 + \gamma(q_i - q_3)^2 - 3k_3^2} \quad (i = 1, 2)\,. \end{aligned} \tag{28}$$

Let

$$\begin{aligned} &p_1 = p_2^* = 1 + i, \quad q_1 = q_2^* = 3 + i, \quad k_3 = 1, \quad p_3 = 2\,, \\ &q_3 = 1, \quad \eta_3^0 = 0, \quad \sigma = -6, \quad \alpha = 1, \quad \beta = \gamma = -1\,. \end{aligned} \tag{29}$$

We derive interaction solutions of Eq. (3) in (x, y) plane, whose dynamical phenomena are exhibited in Fig. 10. At $t = 0$, the peak and valley of the dark lump are divided by the dark soliton and then they keep propagating with the same amplitude, velocity and shape. So, the collision between them is elastic and the other planes have a similar process.

In the case of $N = 4$, with the same method applied above, assuming

$$k_1 = l_1\epsilon, \quad k_2 = l_2\epsilon, \quad k_3 = l_3\epsilon, \quad k_4 = l_4\epsilon, \quad \eta_1^0 = \eta_2^{0*} = \eta_3^0 = \eta_4^{0*} = i\pi\,, \tag{30}$$

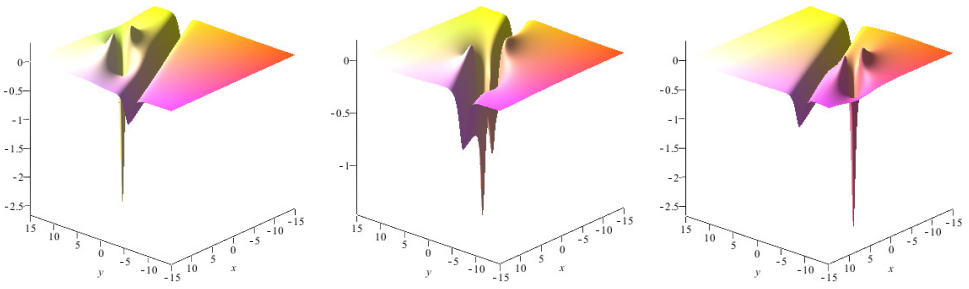

(a) (b) (c)

Fig. 10. (Color online) Elastic collision between dark soliton and dark lump in (x, y) plane with $z = 0$: (a) $t = -1$, (b) $t = 0$ and (c) $t = 1$. Parameters are given in Eq. (29).

it follows:

$$\begin{aligned} f = {} & (\theta_1\theta_2\theta_3\theta_4 + a_{12}\theta_3\theta_4 + a_{13}\theta_2\theta_4 + a_{14}\theta_2\theta_3 + a_{23}\theta_1\theta_4 + a_{24}\theta_1\theta_3 \\ & + a_{34}\theta_1\theta_2 + a_{12}a_{34} + a_{13}a_{24} + +a_{14}a_{23})l_1l_2l_3l_4\epsilon^4 + O(\epsilon^5)\,, \end{aligned} \tag{31}$$

where

$$\begin{aligned} \theta_i &= x + p_i y + q_i z - (\alpha + \beta p_i^2 + \gamma q_i^2)t, \quad i = 1, 2, 3, 4\,, \\ a_{ij} &= \frac{12}{\beta(p_i - p_j)^2 + \gamma(q_i - q_j)^2} \quad (1 \le i < j \le 4)\,. \end{aligned} \tag{32}$$

Let

$$\begin{aligned} p_1 = p_2^* = a_1 + ib_1, \quad q_1 = q_2^* = a_2 + ib_2\,, \\ p_3 = p_4^* = c_1 + id_1, \quad q_3 = q_4^* = c_2 + id_2\,, \end{aligned} \tag{33}$$

where a_i, b_i, c_i, d_i $(i = 1, 2)$ are all real constants. Interaction solutions can be derived with the choices of appropriate parameters. Without loss of generality, setting

$$\begin{aligned} a_1 = \frac{1}{2}, \quad b_1 = \frac{3}{2}, \quad a_2 = 1, \quad b_2 = \frac{1}{2}\,, \\ c_1 = \frac{1}{2}, \quad d_1 = 1, \quad c_2 = 2, \quad d_2 = \frac{3}{2}\,, \end{aligned} \tag{34}$$

we get a nonsingular solution named as two-lump of Eq. (3). Dynamical behaviors in (x, y) plane are visually shown in Fig. 11. In particular, one lump catch up with the stable one and then they collide with each other at $t = 0$, finally they return to the initial state along their original path with the development of time. There is a similar interaction phenomenon between two-lump in other planes.

When $N = 6$, the expression of f contains 76 terms, and it is omitted here due to the limited space. Substituting f into Eq. (5), and taking $p_1 = p_2^*, q_1 = q_2^*$, $p_3 = p_4^*, q_3 = q_4^*, p_5 = p_6^*, q_5 = q_6^*$, we get a nonsingular three-lump solution of Eq. (3). In Fig. 12, the three-lump solution is drawn for a particular choice of the

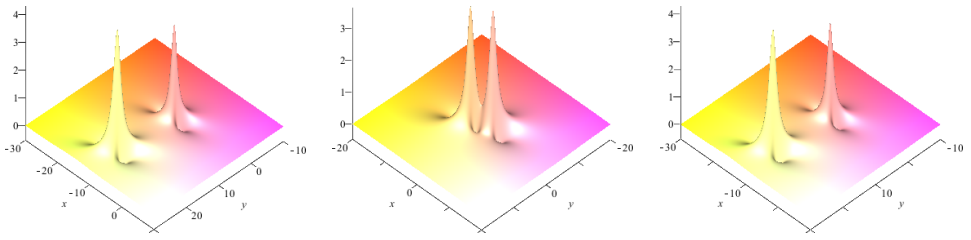

(a) (b) (c)

Fig. 11. (Color online) Elastic collision of two-lump in (x, y) plane. Parameters are constrained in Eq. (34) with $\sigma = 6, \alpha = 1, \beta = \gamma = -1$ and (a) $t = -3$, (b) $t = 0$ and (c) $t = 3$.

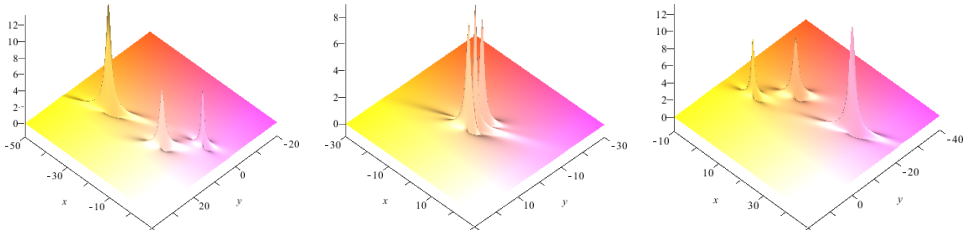

(a) (b) (c)

Fig. 12. (Color online) Elastic collision of three-lump in (x, y) plane with $\sigma = 6, \alpha = 1, \beta = \gamma = -1$ and (a) $t = -1$, (b) $t = 0$ and (c) $t = 1$.

parameters in $p_1 = p_2^* = 2 + i, q_1 = q_2^* = 2 + 3i, p_3 = p_4^* = 1 + 2i, q_3 = q_4^* = 3 + i, p_5 = p_6^* = 1 + i, q_5 = q_6^* = 3 + 2i$.

2.4. *The rogue wave solutions*

In the following, we will construct rogue wave and interaction solutions for the extended KP — Eq. (3). For $N = 2$, when $b_2 = 0$, dark line rogue wave of Eq. (3) can be obtained which comes from a constant background and disappears on a plane. The states of propagation can be seen in Fig. 13(a) with parameters constrained as: $p_1 = p_2^* = 1 + 2i, q_1 = q_2 = 2, \sigma = -6, \alpha = 1, \beta = \gamma = -1$.

In the case of $N = 3$, by assuming $p_1 = p_2^* = 1 + i, q_1 = q_2 = 1, k_3 = 2, p_3 = q_3 = -1, \eta_3^0 = 0, \sigma = -3, \alpha = 1, \beta = \gamma = -1$, interaction solutions between dark soliton and dark line rogue wave will be generated in (x, z) plane. The dynamic features of the interaction solutions are exhibited in Fig. 13(b).

In the case of $N = 4$, two kinds of interaction solutions can be obtained by selecting distinct parameters. When $p_1 = p_2^* = 2 + i, p_3 = p_4^* = 1 + 2i, q_1 = q_2 = 1, q_3 = q_4 = 3, \sigma = -6, \alpha = 1, \beta = \gamma = -1$, two-order dark line rogue wave could be obtained in (x, z) plane. Dynamic phenomena are clearly plotted in Fig. 13(c). When $p_1 = p_2^* = 1 + i, p_3 = p_4^* = 1 + 2i, q_1 = q_2^* = 1 + i, q_3 = q_4 = 2, \sigma = -6, \alpha = 1, \beta = \gamma = -1$, another interaction solutions between dark lump and dark line rogue wave are derived in (x, z) plane. The phenomena of their collision are similar

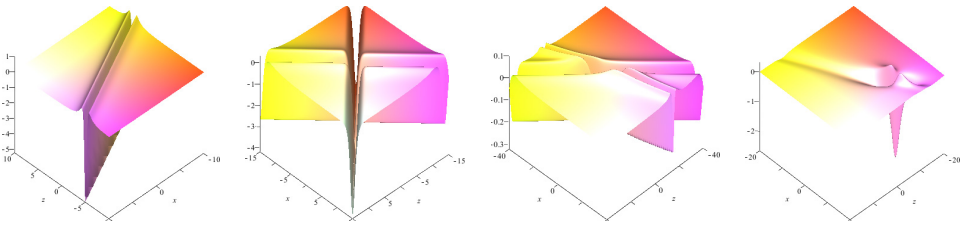

(a) (b) (c) (d)

Fig. 13. (Color online) Graphs of dark line rogue wave and related interaction solutions for f in Eqs. (21), (27) and (31) under transformation (5): (a) $y = 0, t = 0$, (b) $y = 0, t = 0$, (c) $y = 0, t = 1$ and (d) $y = 0, t = 2$.

to the collision between dark soliton and dark line rogue wave which can be seen in Fig. 13(d).

The position and amplitude of dark line rogue cannot be influenced by coefficients α, γ in Eq. (3). However, the amplitude of dark line rogue wave is negative correlation with σ. When mode of β increases, amplitude of the dark line rogue wave increases, but width decreases. For interaction solutions between dark lump and dark line rogue wave, when mode of β increases, amplitude of the dark line rogue wave decreases, but the location keeps unchanged. The location and amplitude of interaction solution are controlled and affected by coefficients α, β and γ.

3. Conclusions

To conclude, four kinds of localized wave solutions of the $(3 + 1)$-dimensional extended KP equation are investigated in this paper. By Hirota bilinear method, the formula of N-soliton solution is constructed and the graphs of explicit one-, two- and three-soliton in (x, y) plane are plotted as an example (see Fig. 1). By the complex conjugate method on multi-soliton solutions, breathers and related interaction solutions are obtained in six different planes. General breathers (see Fig. 2), line breathers (see Fig. 3), interaction solutions between soliton and line breather (see Fig. 4) or general breather (see Figs. 5 and 8) and two-order breathers (see Figs. 6 and 7) are obtained, respectively. Line breathers are periodic line waves and they begin at a constant background and then tend to the original plane, nevertheless general breathers are periodic steady state of wave propagating in one direction. By long wave limit method, lumps and rogue waves are derived by choosing suitable parameters. Lumps and related interaction solutions are exhibited in this paper, including lumps (see Fig. 9), interaction solutions between dark soliton and dark lump (see Fig. 10) in (x, y) plane, interaction solutions of two- and three-lump (see Figs. 11 and 12) in (x, y) plane. In the same way, three types of solutions related with rogue waves are also exhibited in (x, z) plane, including dark line rogue wave (see Fig. 13(a)), interaction solutions between dark soliton and dark line rogue wave (see Fig. 13(b)), interaction solutions of two-order dark line rogue waves (see

Fig. 13(c)), interaction solutions between dark lump and dark line rogue wave (see Fig. 13(d)).

In order to predict the correctness and stability of the localized wave solutions, it is worthy of further exploration to apply numerical simulation method to the above theoretical solutions in the future.

Acknowledgments

The work is supported in part by the National Natural Science Foundation of China under Grant Nos. 11975145, 11271008 and 61072147. The authors would also thank the reviewers for their comments on this paper.

References

1. P. K. Shukla and B. Eliasson, *Phys.-Usp.* **53** (2010) 51.
2. M. S. M. Rajan and A. Mahalingam, *Nonlinear Dynam.* **79** (2015) 2496.
3. M. Savescu, K. R. Khan, P. Naruka, H. Jafari, L. Moraru and A. Biswas, *J. Comput. Theor. Nanosci.* **10** (2013) 1182.
4. X. Lü and W. X. Ma, *Nonlinear Dynam.* **85** (2016) 1217.
5. W. X. Ma, Z. Y. Qin and X. Lü, *Nonlinear Dynam.* **84** (2016) 923.
6. S. F. Tian and P. L. Ma, *Commun. Theor. Phys.* **62** (2014) 245.
7. M. Z. Li, B. Tian, Y. San, X. Y. Wu and C. R. Zhang, *Mod. Phys. Lett. B* **32** (2018) 1850223.
8. N. J. Zabusky and M. D. Kruskal, *Phys. Rev. Lett.* **15** (1965) 240.
9. A. M. Wazwaz and S. A. El-Tantawy, *Nonlinear Dynam.* **84** (2016) 1107.
10. C. C. Ding, Y. T. Gao, L. Hu and T. T. Jia, *Eur. Phys. J. Plus* **133** (2018) 406.
11. J. C. Chen, B. F. Feng, K. I. Maruno and Y. Ohta, *Stud. Appl. Math.* **141** (2018) 145.
12. N. Akhmediev, J. M. Soto-Crespo and A. Ankiewicz, *Phys. Rev. A* **80** (2009) 043818.
13. Z. Y. Yan, *Phys. Lett. A* **375** (2011) 4274.
14. J. S. He, H. R. Zhang, L. H. Wang and A. S. Fokas, *Phys. Rev. E* **87** (2013) 052914.
15. X. Wang, C. Liu and L. Wang, *J. Math. Anal. Appl.* **449** (2017) 1534.
16. W. X. Ma, *Phys. Lett. A* **379** (2015) 1975.
17. M. J. Dong, S. F. Tian, X. W. Yan and L. Zou, *Comput. Math. Appl.* **75** (2018) 957.
18. J. M. Tu, S. F. Tian, M. J. Xu, X. Q. Song and T. T. Zhang, *Nonlinear Dynam.* 83 (2016) 1199.
19. M. Wang, B. Tian, W. R. Shan, X. Lü and Y. S. Xue, *Nonlinear Dynam.* **69** (2012) 1137.
20. H. Y. Ruan and Y. X. Chen, *Phys. Rev. E* **62** (2000) 5738.
21. J. G. Rao, Y. Cheng and J. S. He, *Stud. Appl. Math.* **139** (2017) 568.
22. Y. F. Yue, L. L. Huang and Y. Chen, *Appl. Math. Lett.* **89** (2019) 70.
23. Y. F. Yue and Y. Chen, *Mod. Phys. Lett. B* **33** (2019) 1950101.
24. A. M. Wazwaz, *Appl. Math. Lett.* **64** (2017) 21.
25. J. Satsuma and M. J. Ablowitz, *J. Math. Phys.* **20** (1979) 1496.
26. S. Y. Lou, *Chin. Phys. Lett.* **21** (2004) 1020.
27. W. X. Ma, Y. Zhou and R. Dougherty, *Int. J. Mod. Phys. B* **30** (2016) 1640018.